Soil ozone deposition: Dependence of soil resistance to soil texture

Patrick Stella, Benjamin Loubet, Christophe de Berranger, Xavier Charrier, Eric Ceschia, Giacomo Gerosa, Angelo Finco, Eric Lamaud, Dominique Serça, Christian George, et al.

Soil ozone deposition: dependence of soil resistance to soil texture

P. Stella[1,*], B. Loubet[2], C. de Berranger[3], X. Charrier[3], E. Ceschia[4], G. Gerosa[5], A. Finco[5], E. Lamaud[6], D. Serça[7], C. George[8], R. Ciuraru[2]

[1] UMR SAD-APT, AgroParisTech, INRA, Université Paris-Saclay, 75005, Paris, France
[2] UMR1402 ECOSYS, INRA-AgroParisTech, Université Paris-Saclay, 78850 Thiverval-Grignon, France
[3] INRA UE FERLUS, Les Verrines – CS 80006, 86600 Lusignan, France
[4] CESBIO, UMR 5126 – CNES-CNRS-UPS-IRD – 18 avenue Edouard Belin 31401 Toulouse cedex 9, France
[5] Dipartimento di Matematica e Fisica, Università Cattolica del Sacro Cuore, via Musei 41, 25121 Brescia, Italia
[6] UMR 1391 ISPA, INRA-Bordeaux Sciences Agro, F-33140 Villenave d'Ornon, France
[7] Laboratoire d'Aérologie, Université de Toulouse, CNRS, UPS, France
[8] Université de Lyon 1 CNRS, UMR5256, IRCELYON, Institut de Recherches sur la Catalyse et l'Environnement de Lyon, F-69626 Villeurbanne, France
[*] Correspondence to: P. Stella (patrick.stella@agroparistech.fr)

Abstract

Soil deposition is an essential pathway for tropospheric ozone (O_3) removal, but its controlling factors remain unclear. Here, we explored the variability of soil O_3 resistance in response to soil texture. To this aim, data of O_3 deposition over bare soil obtained from micrometeorological measurements under contrasted meteorological conditions for five sites were used. The results obtained are twofold: (i) soil resistance (R_{soil}) increased with soil surface relative humidity (RH_{surf}), but (ii) this relationship exhibited large site-by-site variability. Further analysis showed that the minimum soil resistance (corresponding to completely dry soil surface or RH_{surf} = 0%) and the increase of R_{soil} with RH_{surf} are both linked to soil clay content. These results can be explained by (i) the soil surface available for O_3 deposition at a microscopic scale which is a function of the soil specific surface area, and (ii) the capacity of a soil to adsorb water according to its clay content and therefore to reduce the surface active for O_3 deposition. From these results, a new parameterization has been established to estimate R_{soil} as a function of RH_{surf} and soil clay fraction.

Keywords: Ozone; soil resistance; clay content; relative humidity.

1 – INTRODUCTION

Since the pre-industrial era, concentrations of tropospheric ozone (O_3) have sharply increased in the atmosphere. It is a well-known greenhouse gas responsible for a positive radiative forcing of 0.40 W m^{-2} i.e., around 20% of the total radiative forcing attributed to human activities, and the largest contributor to radiative forcing after long-lived trace gases (CO_2, N_2O, CH_4, and halocarbons) (IPCC, 2013). Yet, due to its oxidative capacity, O_3 is also a key compound in atmospheric chemistry (Monks, 2005) and a widespread secondary pollutant. It is responsible for the oxidation of numerous compounds (e.g., Lee et al., 1996; Ahmad et al., 2000) and for negative impacts on human health (Ito et al., 2005; Hazucha and Lefohn, 2007; Doherty et al., 2017). On terrestrial ecosystems, O_3 penetrates through plant stomata and induces a range of metabolic changes such as a decrease of photosynthetic capacity, alteration of plant biomass and structure, stomatal closure, and acceleration of senescence (e.g., Karnosky et al., 2003; Paoletti, 2005; Felzer et al., 2007; Dizengremel et al., 2008; Booker et al., 2009; Wittig et al., 2009; Ainsworth et al. 2012, Lombardozzi et al., 2013). All these alterations lead to the decrease of ecosystem productivity and crop yield losses (e.g., Ainsworth et al., 2012; Lombardozzi et al., 2015; Franz et al., 2017), which in turn could contribute indirectly to global warming due to the alteration of global carbon cycle (Felzer et al., 2007; Sitch et al., 2007).

Since O_3 is weakly soluble in water, it is mainly deposited through dry deposition on terrestrial ecosystems (Fowler et al., 2009), which is the only net removal pathway of O_3 from the atmosphere and therefore an important process governing the tropospheric O_3 budget (Stevenson et al., 2006; Wild, 2007). Many studies have been carried out over natural ecosystems and agroecosystems in order to (i) understand the processes governing O_3 dry deposition, (ii) establish parameterizations for O_3 deposition, and (iii) quantify the terrestrial O_3 sink (e.g., Zhang et al., 2006; Coyle et al., 2009; Lamaud et al., 2009; Stella et al., 2011a, 2013; Fares et al., 2012; Launiainen et al., 2013; Clifton et al., 2017; Freire et al., 2017). Deposition occurs through stomatal and non-stomatal (i.e., soil and cuticular) pathways. Due to their dependence on leaf area index (LAI), O_3 deposition mainly occurs through stomatal and cuticular pathways on fully developed canopies, while transfer from the atmosphere toward the ground is reduced when the canopy height and LAI increase (van Pul and Jacobs, 1994; Zhang et al., 2002; Massman, 2004; Tuovinen et al., 2004; Stella et al., 2011a, 2013). Hence, strong efforts have been done to understand the processes governing stomatal (e.g., Emberson et al., 2000) and cuticular deposition (e.g., Zhang et al., 2002; Altimir et al., 2004,

2006; Coyle et al., 2009; Cape et al., 2009; Lamaud et al., 2009; Potier et al., 2015), although these processes are still not well described and no consensual parameterization exists.

Over fully developed canopies, soil deposition is the smallest contributor to total deposition and processes governing this deposition pathway received little attention. Nevertheless, it cannot be neglected for short or sparse canopies, and of course during bare soil periods. Yet, Stella et al. (2013) reported that soil O_3 deposition was the main deposition pathway and represented 55% of the total O_3 deposition over an agricultural field for a 2 year period.

Few studies have investigated the processes governing soil deposition. Some authors associated soil O_3 resistance (R_{soil}) to soil water content (e.g., Bassin et al., 2004; Massman, 2004; Meszaros et al., 2009), but the suggested parameterizations are not able to correctly estimate O_3 deposition during bare soil or growing season periods (Stella et al., 2011b, 2013). From measurements carried out over bare soil, Stella et al. (2011b) showed that R_{soil} was linked to soil surface relative humidity (RH_{surf}), but the relationships proposed seems to be site-dependent (Stella et al., 2011a).

This study aims now to explore the relationships between R_{soil} and RH_{surf} and its dependence on soil texture, with data obtained only over bare soil are used. A new parameterization of R_{soil} accounting for soil texture is proposed.

2 – MATERIAL AND METHODS

2.1 – Site descriptions, datasets, and measurements

Standard meteorological variables (i.e., global radiation (R_g), wind speed (u), air temperature (T_a), air relative humidity (RH_a) as well as turbulent fluxes (sensible (H) and latent (LE) heat fluxes, and momentum (τ) flux from which is deduced friction velocity (u_*)) and O_3 deposition velocities (V_d) measured by the eddy-covariance method were collected over five different sites during bare soil periods. Site, experimental set-up, and data processing were already described in previous studies for La Crau (Michou et al., 2005), Lamasquère (Béziat et al., 2009; Stella et al., 2011a), and La Cape Sud (Stella et al., 2009, 2011a).

The first dataset was collected between 20 April and 31 May 2001 in the semi-arid part of the La Crau plain, France (43°34'N, 4°49'E). The site consisted of an almost bare soil with mainly pebbles. Ozone fluxes were measured by eddy-covariance with a fast-response O_3 chemiluminescent analyzer (OS-G-2, Güsten, 1992). Its calibration was continuously checked against a slow-response O_3 monitor (O_3 41M, Environnement SA, FR).

The second dataset corresponds to measurements performed during four bare soil periods (24 April 2008 to 26 May 2008, 20 November 2008 to 18 December 2008, 14 November 2009 to 12 May 2010, 29 September 2010 to 9 November 2010) over an agricultural field located at Lamasquère, 20 km south-west of Toulouse, France (43°49'N, 1°23'E). Ozone deposition was assessed by eddy-covariance using a fast-response O_3 chemiluminescent analyzer (ATDD, NOAA, USA). Owing to the very small and constant offset of the O_3 analyzer, direct measurement of V_d was provided following the ratio method described in Müller et al. (2010).

The third dataset concerns measurements carried out over an agricultural field during bare soil period at La Cape Sud, 60 km south of Bordeaux, France (44°24'N, 0°38'W), from 19 October 2007 to 4 March 2008. As for Lamasquère, O_3 deposition velocity was measured by eddy-covariance following the ratio method (Müller et al., 2010) by using a fast-response O_3 chemiluminescent analyzer (ATDD, NOAA, USA).

The fourth dataset was collected from 17 March to 5 May 2011 over an agricultural field during bare soil period before maize sowing at Lusignan site, 30 km south of Poitier, France (46°24'N, 0°07'E). Standard meteorological conditions were measured at 1.86 m above ground level (a.g.l.) including net, incident and reflected shortwave, and incident and reflected longwave radiations (CNR1, Kipp & Zonnen, NL), air temperature and relative humidity (HMP45C, Vaisala, FI), wind speed (A100R, Campbell Scientific, USA), wind direction (W200P, Campbell Scientific, USA), and rainfall (SBS500, Campbell Scientific, USA). Soil temperatures were measured at 0.05, 0.10, 0.20, 0.30, 0.60, 0.80, and 1m depth using PT100 sensors (Mesurex, FR), as well as soil water content at 0.10, 0.20, 0.30, 0.60, 0.80 and 1m depth with CS616 probes (Campbell Scientific, USA). Soil heat flux was measured with two flux plates (HFP01, Hukseflux, NL). All microclimatic data were sampled every 30 s on data logger (CR1000, Campbell Scientific, USA) and averaged every 30 min. Turbulent fluxes of momentum, sensible heat, water vapor, CO_2 and O_3 were measured at 1.86 m a.g.l. by eddy-covariance (EC). The EC system consisted in a 3D sonic anemometer (R3-50, GILL Instruments, UK) coupled with CO_2/H_2O Infrared Gas Analyzer (LI-7500, LICOR, USA), and a fast-response O_3 chemiluminescent analyzer (ATDD, NOAA, USA). The coumarin dye of the fast-response O_3 analyzer was changed once per week. Data were sampled and recorded at 20 Hz on a computer using Edisol software (University of Edinburgh, UK), and flux integration was performed over 30 min time spans. Flux calculation was assessed following the CarboEurope methodology (Aubinet et al., 2000). In the case of O_3, the ratio method providing deposition velocity (Muller et al., 2010) was applied.

The last dataset corresponds to measurements performed between 24 March to 14 April 2014 at Turro (PC) Italy, (44°59'N, 9°42'E) (Scalvenzi, 2015). The site consisted in an agricultural field with bare, ploughed and smoothed soil. Standard meteorological conditions were measured 2.2 m a.g.l.: net radiation (NR-LITE, Kipp & Zonen, NL), incident solar radiation (LI 200 SZ, LI-COR, USA), and air temperature and humidity (HD9000, Deltaohm, I). Soil heat fluxes (HFP01, Hukseflux, NL) were measured at 0.05 m depth while soil water content (CS616, Campbell Scientific, USA) was measured with a reflectometer averaging the soil water content in the first 30 cm of soil below ground. All the data from these probes were averaged each half an hour and collected on a data logger (CR10x, Campbell Scientific, USA). An additional mast was set up for wind speed, wind direction and eddy covariance flux measurements at 2.2 m a.g.l., and included an ultrasonic anemometer (USA-1, Metek, D), a krypton hygrometer (KH2O, Campbell Scientific, USA), and a fast-response chemiluminescent O_3 analyser (COFA, Ecometrics, I) based on the reaction between ozone and coumarin for which the dye was changed typically every 5 days. An additional slow response photometric O_3 analyser (1308, SIR, E) was used to calibrate the fast-response O_3 analyser. Eddy covariance data were recorded at 10 Hz and collected on a personal computer and stored in half an hour files. Flux calculation was assessed following the CarboEurope methodology (Aubinet et al., 2000) and included raw data despiking following the procedure proposed by Vickers and Mahrt (1997), linearly gap-filling, and a double rotation of the reference system of the wind components (Wilczak et al., 2001).

2.2 – Calculation of ozone soil resistance and surface relative humidity

Following the resistance analogy (Wesely and Hicks, 2000), V_d (in m s^{-1}) to bare soil is expressed as:

$$V_d = \frac{1}{R_a(z)+R_{bO3}+R_{soil}} \quad (1)$$

where R_{soil} (s m^{-1}) is the soil resistance, and $R_a(z)$ and R_{bO3} (s m^{-1}) are the aerodynamic and the quasi-laminar boundary layer resistances, respectively, calculated following Garland (1977). From Eq. (1), R_{soil} is expressed as:

$$R_{soil} = V_d^{-1} - R_a(z) - R_{bO3} \quad (2)$$

According to Stella et al. (2011b), R_{soil} depends on surface air relative humidity (RH_{surf} in %) at $z_{0'}$ (soil roughness height for scalar):

$$R_{soil} = R_{soil\,min} \times exp^{(k \times RH_{surf})} \quad (3)$$

where $R_{soil\ min}$ (s m^{-1}) is the soil resistance without water adsorbed at the surface (i.e. at RH_{surf} = 0%) and k is an empirical coefficient of the exponential function.

Following Stella et al. (2011b), RH_{surf} is retrieved from H and LE by using the resistance analogy:

$$T_{surf} = \frac{H\,(R_a(z)+R_b)}{\rho\ C_p} + T_a \quad (4)$$

$$\chi_{H2Osurf} = E(R_a(z) + R_{bH2O}) + \chi_{H2Oa} \quad (5)$$

$$P_{vapsurf} = \frac{\chi_{H2Osurf}\,R\,(T_{surf}+273.15)}{M_{H2O}} \quad (6)$$

$$P_{sat}(T_{surf}) = p\ exp\left[\frac{M_{H2O}\ 10^{-3}\ L}{R}\left(\frac{1}{T_0+273.15} - \frac{1}{T_{surf}+273.15}\right)\right] \quad (7)$$

$$RH_{surf} = \frac{P_{vapsurf}}{P_{sat}(T_{surf})} \times 100 \quad (8)$$

with T_{surf} the surface temperature (°C), ρ the air density (kg m^{-3}), C_p the air specific heat (J kg^{-1} K^{-1}), $\chi_{H2Osurf}$ and χ_{H2Oa} the air concentration of water (g m^{-3}) at z_0, and reference height, respectively, E the water vapor flux (kg m^{-2} s^{-1}), $P_{vapsurf}$ the water vapor pressure at z_0, (Pa), R the universal gas constant (J mol^{-1} K^{-1}), M_{H2O} the molecular weight of water (g mol^{-1}), $P_{sat}(T_{surf})$ the saturation vapor pressure at T_{surf} (Pa), p the atmospheric pressure (Pa), L the latent heat of vaporization of water (J kg^{-1}), and T_0 the boiling temperature of water (°C).

3 – RESULTS AND DISCUSSION

3.1 – Weather, pedoclimate and ozone deposition

Meteorological variables followed typical diurnal trends at each sites. Global radiation and u_* increased in early morning to reach their maximum at around noon and then decreased to their minimum in late afternoon (Figures 1a and 1d). Air temperature and RH_a exhibited opposite trends: while the former increased in early morning to reach its maximum in early afternoon and then decreased (Figure 1b), the latter decreased until early afternoon to its minimum value before increasing to its maximum occurring during nighttime (Figure 1c). Soil water content did not show marked diurnal trend for the three sites where it was measured (i.e., Lamasquère, Lusignan, and Turro) (Figure 1e).

Although diurnal trends of meteorological variables were similar, pedoclimatic conditions were contrasted at each site. La Crau exhibited the sunniest and warmest meteorological conditions with mean R_g=232 W m^{-2} over the whole experimental period (Table 1), and

maximum half hourly R_g around 730 W m^{-2} (Figure 1a). Air temperature and relative humidity were on average at 15.8°C and 72% (Table 1) with maximum and minimum half-hourly means around 19°C / 85% and 12°C / 54%, respectively (Figure 1b and 1c). The highest u_*, due to windy conditions typical of Mistral in this region, was also recorded on this site: 0.30 m s^{-1} on average (Table 1) and varied between 0.2 m s^{-1} during nighttime and 0.43 m s^{-1} during daytime (Figure 1d). The soil type was loam (22% clay, 36% silt, 38% sand) but the soil surface was mainly composed of pebbles. Rainfall and SWC were not recorded on this site. At Lamasquère, R_g averaged 281 W m^{-2} for the whole dataset (Table 1) and its mean half hourly value peaked at 415 W m^{-2} (Figure 1a). Half hourly means of T_a and RH_a ranged between 6°C and 90% during nighttime and 13°C and 65% during daytime (Figure 1b and 1c), and averaged 9.2°C and 79% over the whole dataset (Table 1), respectively. Mean u_* was at 0.21 m s^{-1} (Table 1) over the whole dataset and ranged from 0.16 m s^{-1} during nighttime and 0.29 m s^{-1} during daytime (Figure 1d). During the 281 days of the dataset, 833 half hourly rainfall events were recorded, representing 544 mm cumulated and on average 0.65 mm per rainfall event. The soil type was clay (54% clay, 34% silt, 12% sand) with a mean SWC of 38% (Table 1). Weather at La Cape Sud was characterized by cloudy and cold conditions: R_g and T_a were the lowest of the five datasets, with averages over the whole dataset at 68 W m^{-2} and 6.2°C (Table 1), and half hourly means ranging from 0 to 273 W m^{-2} and from 2.5 to 12°C (Figure 1a and 1b), respectively. Dry atmospheric conditions were measured: although RH_a averaged 73% (Table 1), it decreased to 50% during daytime and reached 85% during nighttime (Figure 1c). Friction velocity ranged between 0.1 and 0.25 m s^{-1} (Figure 1d), with mean u_* of 0.15 m s^{-1} (Table 1). Cumulated rainfall during the 137 days of the dataset was at 177 mm, and 365 half hourly events of 0.48 mm on average occurred. The soil type at this site was loamy sand (6% clay, 9% silt, 77% sand) (Table 1). At Lusignan, half hourly mean R_g peaked at 600 W m^{-2} (Figure 1a) and averaged 195 W m^{-2} over the whole dataset (Table 1). Means of T_a and RH_a were at 12.6°C and 69% (Table 1) and their half hourly means ranged from 7.5°C to 17.7°C (Figure 1b) and from 87% to 50% (Figure 1c), respectively. This dataset exhibited the weakest u_* and SWC: they were on average at 0.13 m s^{-1} and 27%, respectively (Table 1). Half hourly means of u_* only varied from 0.09 m s^{-1} during nighttime to 0.20 m s^{-1} during daytime (Figure 1d), while half hourly means SWC did not show diurnal variations (Figure 1e). Cumulated rainfall during the 49 days of the dataset was at 36 mm, and 63 half hourly events of 0.59 mm on average occurred. The soil type at this site was silt loam (17% clay, 60% silt, 23% sand) (Table 1). The last site, Turro, presented intermediate R_g: it was on average over the whole dataset 155 W m^{-2} (Table 1) and its half hourly mean peaked

227 to 516 W m^{-2} (Figure 1a). Half hourly means of T_a were similar to those recorded at Lusignan
228 during nighttime and La Crau during daytime, i.e., ranged from 7.5°C to 19°C (Figure 1b).
229 Over the whole dataset, T_a was on average at 13.3°C (Table 1). For RH_a, half hourly means
230 varied between 90% and 60% and was 77% over the whole dataset (Figure 1c and Table 1).
231 The friction velocity exhibited quite large diurnal variation: its half hourly means ranged from
232 0.1 m s^{-1} during nighttime to 0.37 m s^{-1} during daytime (Figure 1d) while it was on average at
233 0.21 m s^{-1} during the whole measurement period (Table 1). This site exhibited the largest
234 SWC, 42% (Table 1). During the 21 days of the dataset, 55 half hourly rainfall events were
235 recorded, representing 35.6 mm cumulated and on average 0.65 mm per rainfall event. The
236 soil type was silty clay loam (30% clay, 52% silt, 18% sand) (Table 1).

237 Half hourly means of V_d are presented in Figure 1f. Excepted at Turro, V_d measured during
238 nighttime was similar at each site, between 0.15-0.25 cm s^{-1}. They then increased during early
239 morning to reach their maximum, around 0.30 cm s^{-1} at La Crau, 0.40 cm s^{-1} at Lamasquère
240 and La Cape Sud, and 0.60 cm s^{-1} at Lusignan. At Turro, V_d did not follow typical diurnal
241 dynamics and exhibited important half-hourly variations, with half hourly V_d oscillating
242 around 0.5-0.6 cm s^{-1} during both nighttime and daytime, and exhibiting two peaks (at around
243 1-1.2 cm s^{-1}) during early morning and late evening. As a consequence, with
244 0.61 cm s^{-1}, V_d was on average over the whole dataset the largest at this site. For the other
245 sites, mean V_d was 0.21 cm s^{-1} for La Crau, 0.29 cm s^{-1} for Lamasquère, 0.26 cm s^{-1} for La
246 Cape Sud, and 0.36 cm s^{-1} for Lusignan (Table 1).

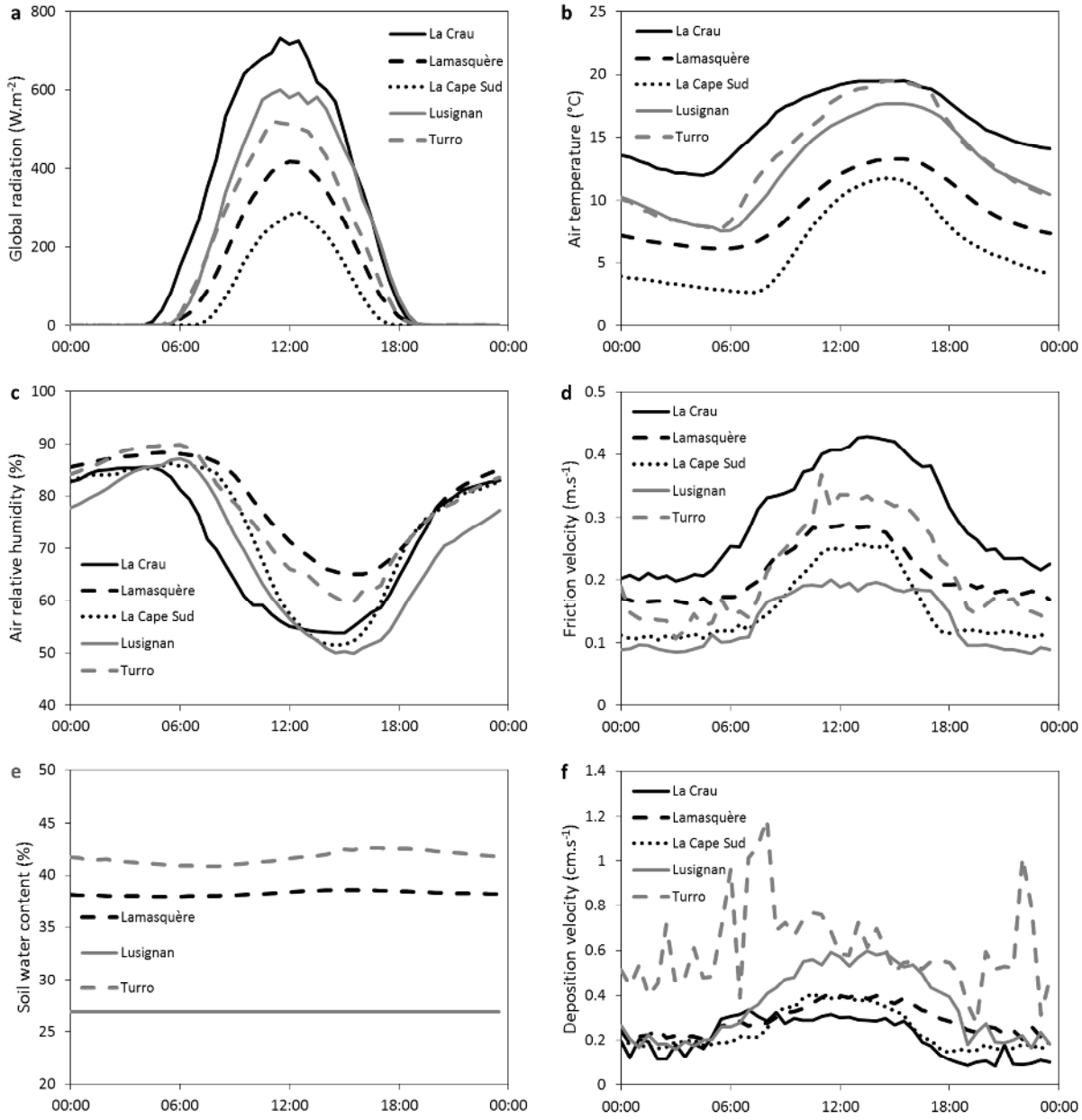

Figure 1: Half hourly arithmetic means of **(a)** global radiation, **(b)** air temperature, **(c)** air relative humidity, **(d)** friction velocity, **(e)** soil water content, and **(f)** deposition velocity for La Crau (black line), Lamasquère (dashed black line), La Cape Sud (dotted black line), Lusignan (grey line), and Turro (dashed grey line) sites.

Table 1: Arithmetic means (± standard deviations) of global radiation (R_g), air temperature (T_a), air relative humidity (RH_a), friction velocity (u_*), rainfall, soil water content (SWC), and deposition velocity (V_d) during the measurement periods for each site. Are also indicated the dataset duration, cumulated rainfall, number of half hourly rainfall events (n), and soil texture.

	Dataset duration	R_g	T_a	RH_a	u_*	**Rainfall**			**SWC**	**Soil texture**	V_d
	Days	W m^{-2}	°C	%	m s^{-1}	mm			%	%Clay %Silt %Sand	cm s^{-1}
		Mean ± SD	Mean ± SD	Mean ± SD	Mean ± SD	Mean ± SD	Sum	n	Mean ± SD		Mean ± SD
La Crau	41	232±298	15.8±4.5	72±19	0.30±0.20	-	-	-	-	22* 36* 38*	0.21±0.21
Lamasquère	281	118±207	9.2±6.5	79±15	0.21±0.16	0.65±0.86	544	833	38±4	54 34 12	0.29±0.33
La Cape Sud	137	68±118	6.2±5.3	73±19	0.15±0.12	0.48±0.49	177	365	-	6* 9* 77*	0.26±0.20
Lusignan	49	195±261	12.6±4.9	69±20	0.13±0.09	0.59±0.74	36	63	27±1	17 60 23	0.36±0.28
Turro	21	155±209	13.3±4.5	77±13	0.21±0.11	0.65±0.83	35.6	55	42±3	30 52 18	0.61±0.48

*: Not measured on site, obtained from Geosol Database (http://estrada.orleans.inra.fr/geosol/).

3.2 – Relationships between R_{soil} and RH_{surf}

Several authors related R_{soil} to the amount of water in soil, and showed that the drier the soil is, the weaker R_{soil} is (e.g., Bassin et al., 2004; Massman, 2004; Meszaros et al., 2009). More recently, Stella et al. (2011b) showed that (i) the estimate of R_{soil} as a function of soil water content does not provide an accurate estimate of V_d over bare soil, and (ii) R_{soil} depends on and increases exponentially with RH_{surf}. Therefore, the relationships between R_{soil} and RH_{surf} were determined for each site and are presented in Figure 2. From these relationships, the two parameters of the exponential function controlling R_{soil} i.e., $R_{soil\ min}$ and k (Equation 3), were

estimated from the exponential regression between R_{soil} and RH_{surf} (Figure 2), and are summarized in Table 2.

Whatever the site considered, R_{soil} increases exponentially with RH_{surf}. These results confirm those previously obtained by Stella et al. (2011b) at an agricultural field during bare soil periods. Nevertheless, this relationship substantially differs quantitatively according to the site considered, as shown in Figure 2 and by the values obtained for $R_{soil\ min}$ and k (Table 2).

The minimum resistance i.e., R_{soil} at RH_{surf} = 0% corresponding to $R_{soil\ min}$, strongly varied according to the site considered (Figure 2 and Table 2). The lowest resistance was observed at Lamasquère (12 ± 1.20 $s.m^{-1}$) and the largest at La Crau (169 ± 1.18 $s\ m^{-1}$). For Lusignan, Turro, and La Cape Sud, $R_{soil\ min}$ was 29 ± 1.01 $s\ m^{-1}$, 42 ± 1.22 $s\ m^{-1}$, and 161 ± 1.11 $s\ m^{-1}$, respectively. As far we know, only two studies reported values of $R_{soil\ min}$. The first concerns the study of Stella et al. (2011b) for an agricultural field during bare soil periods who found $R_{soil\ min}$ = 21 ± 1.01 $s\ m^{-1}$. The second originated from Güsten et al. (1996) who reported from an experiment in Sahara desert an average daytime resistance of ozone to desert sand of 800 $s.m^{-1}$. In such conditions, it can be hypothesized that RH_{surf} is very close or equal to 0%, and hence the value reported by Güsten et al. (1996) corresponds to $R_{soil\ min}$. Therefore, in spite of their large range of variation, the values found for our five sites remain in the range reported by previous studies.

Similarly to $R_{soil\ min}$, the increase of R_{soil} with RH_{surf}, corresponding to k, exhibited large site-by-site variations (Figure 2 and Table 2). The slowest increase was found at La Crau and La Cape Sud, with k equal to 0.017 ± 0.003 and 0.013 ± 0.002, respectively, while Lamasquère exhibited the fastest increase (k = 0.055 ± 0.003). The values found at Lusignan and Turro were intermediate, 0.025 ± 0.001 and 0.021 ± 0.003, respectively, but are similar to the one reported by Stella et al. (2011b) who reported k = 0.024 ± 0.001.

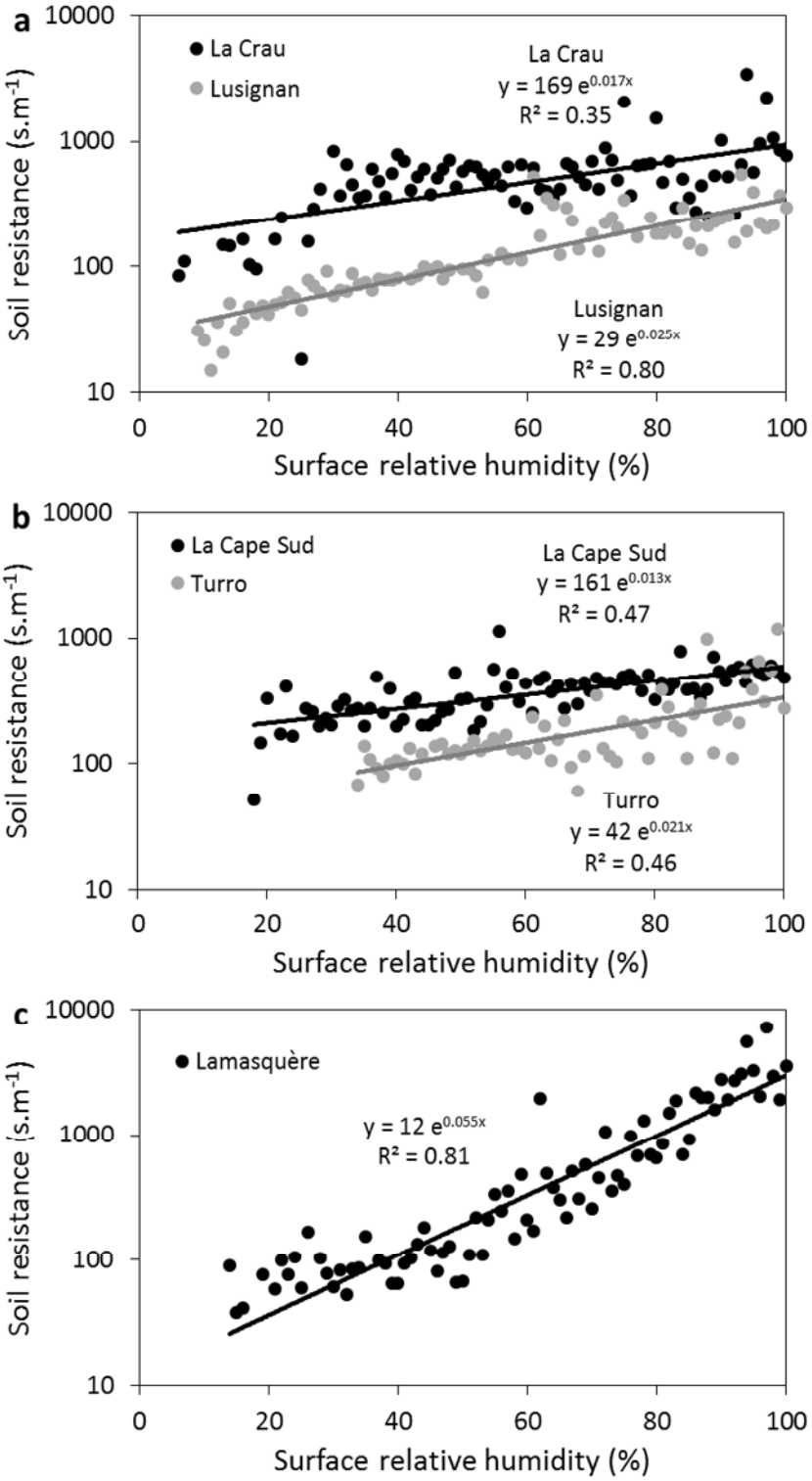

Figure 2: Soil resistance as a function of surface relative humidity for **(a)** La Crau (black symbols) and Lusignan (grey symbols), **(b)** La Cape Sud (black symbols) and Turro (grey symbols), and **(c)** Lamasquère. Data are block averaged with a range of 1% surface relative humidity. Lines represent the regression (general form: $R_{soil} = R_{soil\,min} \times exp^{(k \times RH_{surf})}$). Only data for $u_* > 0.1$ m s^{-1} were used.

298 **Table 2:** Minimum soil resistances ($R_{soil\ min}$), empirical coefficients of the exponential
299 functions (k) and clay contents obtained for the sites of this study. The values and their
300 standard errors were obtained by the regressions between R_{soil} and RH_{surf}. Are also indicated
301 the values reported by Stella et al. (2011b) and Gusten et al. (1996) (see text for details).

	$R_{soil\ min}$	k	Clay content
	$s.m^{-1}$	-	%
	Value ± SE	Value ± SE	
Lamasquère	12 ± 1.20	0.055 ± 0.003	54
Stella et al. (2011b)[1]	21 ± 1.01	0.024 ± 0.001	31
Lusignan	29 ± 1.01	0.025 ± 0.001	17
Turro	42 ± 1.22	0.021 ± 0.003	30
La Cape Sud	161 ± 1.11	0.013 ± 0.002	6
La Crau	169 ± 1.18	0.017 ± 0.003	22
Güsten et al. (1996)[2]	800	[-]	0.8

302 [1] Soil texture: 31% Clay, 62.5% Silt, 6.5% Sand

303 [2] Soil texture: 0.8% Clay, 1.3% Silt, 97.9% Sand

304 **3.3 – Dependence of R_{soil} parameters to soil texture**

305 As shown previously, the dependence of R_{soil} to RH_{surf} exhibits large site-by-site variations, as
306 suggested by Stella et al. (2011a, 2011b). Yet, Stella et al. (2011b) hypothesized that the
307 increase of R_{soil} with RH_{surf} is due to the presence of water adsorbed at the soil surface,
308 decreasing the surface active for O_3 deposition since O_3 is hardly soluble in water i.e., R_{soil}
309 depends on the available dry soil surface.

310 In our study, the main difference that could explain this variability between each site concerns
311 the soil texture, which would be consistent with the hypothesis proposed by Stella et al.
312 (2011). Indeed, the soil texture and more specifically the clay content determines the specific
313 surface area i.e., the mass normalized surface area (in $m^2\ g^{-1}$): at a microscopic scale the
314 surface for the same amount of soil increases with clay content due to the size and structure of
315 these elements. This issue has been proved both theoretically and experimentally in e.g.,
316 Petersen et al. (1996) and Pennel (2002). In other words, the greater the amount of clay is, the

larger the surface available at a microscopic scale for O_3 deposition is. To examine this issue, the two parameters $R_{soil\ min}$ and k were plotted as a function of soil clay content.

The results are presented in Figure 3 and include those obtained from the sites of this study as well as those from Güsten et al. (1996) and Stella et al. (2011b). The results from La Crau were not included in fitting the relationships between $R_{soil\ min}$ and k and the soil clay content, as discussed at the end of this section. On the one hand, $R_{soil\ min}$ decreases when soil clay content increases. This decrease is particularly marked for soil clay content lower that 10-15%. Above this percentage, $R_{soil\ min}$ decreases less rapidly. The best correlation coefficient was obtained for a power regression ($R_{soil\ min} = 702 \times (clay\ content)^{-0.98}$; $R^2 = 0.95$) (Figure 3a). On the other hand, k increases with soil clay content and the best correlation coefficient was found for an exponential relationship ($k = 0.0118 \times exp^{-0.0266 \times (clay\ content)}$; $R^2 = 0.85$) (Figure 3b).

As expected from our working hypothesis, when there is no water adsorbed at the soil surface the soil resistance (i.e., $R_{soil\ min}$) decreases with the increase in soil clay content. In other words, O_3 deposition to soil is favored when the soil specific surface increases, since more surface is available for O_3 removal at a microscopic scale. As far we know, only the study of Sorimachi and Sakamoto (2007) has already examined in this issue with similar results. From laboratory measurements of O_3 deposition onto different soil samples, they reported that for soil moisture content lower than 10% (i.e., close to RH_{surf}) the surface resistance decreases exponentially with increasing soil surface area. Nevertheless, it must be noted that from our in-situ measurements it was found a power decrease instead of an exponential one. Concerning the increase of k with soil clay content, a possible explanation would be link to the capacity of a soil to adsorb/desorb water, and therefore to contain water, according to its amount of clay. According to Schneider and Goss (2012), for the same relative humidity, the water content is larger for soil with a large amount of clay than for soil with low amount of clay. In addition, its increase with relative humidity is faster when the amount of clay is large. Since O_3 is hardly soluble in water, this statement could explain the faster increase of R_{soil} with RH_{surf} (i.e. larger k) for soils with larger clay content.

Results obtained at La Crau site exhibited discrepancies compared to the results obtained on the other sites, especially concerning $R_{soil\ min}$ (Figure 3a). For this latter, there are only two possibilities: (i) $R_{soil\ min}$ is underestimated or (ii) the soil clay content is overestimated. The former seems not to be plausible since the methodology to deduce $R_{soil\ min}$ is identical for all the sites. However, it is possible that the percentage of clay did not reflect reality. Since O_3 is

an highly reactive compound, it can be rapidly depleted. Therefore, properties retained must be representative of the soil surface, i.e., the first few millimeters. At this site, soil surface was mainly composed of pebbles for which specific surface is small. Thus the "real clay content" of the soil surface at this site, in regards with soil specific surface area, would be probably closer to a sandy soil as for La Cape Sud, for which both $R_{soil\ min}$ and k are similar with the La Crau ones (Table 2).

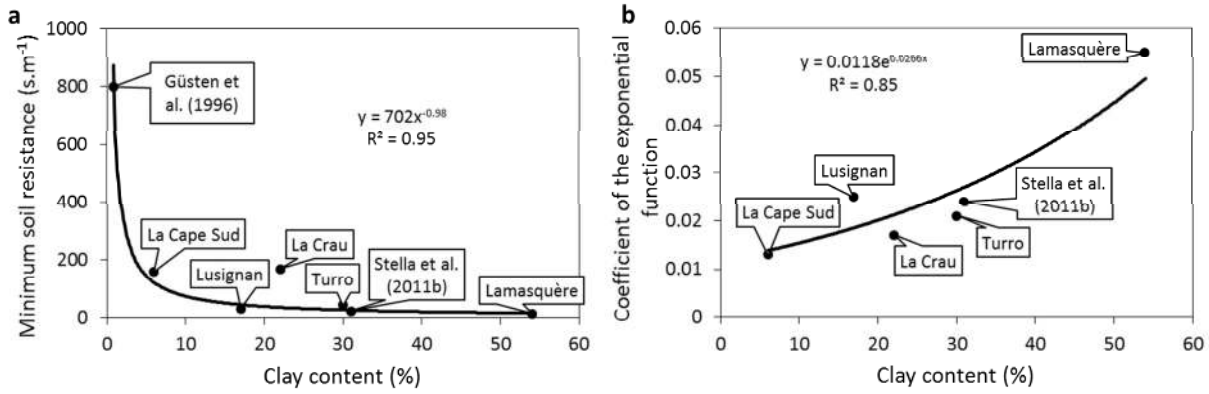

Figure 3: Relationships between **(a)** minimum soil resistance ($R_{soil\ min}$) and **(b)** coefficient of the exponential function (k) and soil clay content. Black lines correspond to the regressions. Values from La Crau site were not included in the regressions.

4 – CONCLUSIONS AND PERSPECTIVES

This study explored the variability of soil O_3 resistance according to soil texture. To this end, O_3 deposition data over bare soil obtained from micrometeorological measurements under contrasted meteorological conditions for five sites were used. The results obtained are twofold: (i) R_{soil} increases with RH_{surf} as found previously by Stella et al. (2011b), but (ii) the relationships exhibited large site-to-site variability. From the data analysis, the minimum soil resistance without water adsorbed at the surface (i.e., at RH_{surf} = 0%) corresponding to $R_{soil\ min}$, and the increase of R_{soil} with RH_{surf} corresponding to k are linked to soil clay content. These patterns can be explained respectively by (i) the surface available for O_3 deposition at a microscopic scale which is linked to the soil specific surface area, and (ii) the capacity of a soil to adsorb water according to its clay content and therefore to reduce the surface active for O_3 deposition. From our results (Figure 3) a new parameterization can be established to estimate R_{soil} as a function of RH_{surf} (%) and soil clay content (%):

$$R_{soil} = 702 \times (clay\ content)^{-0.98} \times exp^{(0.0118 \times exp^{(-0.0266 \times (clay\ content)} \times RH_{surf})} \quad (9)$$

374 This empirical parameterization could be included into surface-atmosphere exchanges models
375 to assess the O_3 dry deposition budget of continental surface since (i) the soil component can
376 represent an important fraction of total deposition especially for agroecosystems (Stella et al.
377 2013) and (ii) current parameterizations accounting for soil water content overestimate R_{soil},
378 especially under dry conditions (Stella et al., 2011b). For instance, assuming a soil water
379 content equal to 0%, the parameterization used in Bassin et al. (2004) and Meszaros et al.
380 (2009) gives R_{soil} = 200 s.m^{-1}, values that are particularly high compared to the smallest ones
381 deduced at Lusignan, Lamasquère and Turro (Figure 2).

382 It must however be noted that our study is limited to only few sites. Ozone deposition is rarely
383 measured over bare soil, and further efforts should be done to complete our study and assess
384 the relationships proposed. Yet, we limited our study to the soil texture which is the main
385 factor controlling the soil specific surface area, but other parameters also modify it, such as
386 soil compaction. In addition, we only focused our work on the hypothesis of a physical
387 underlying process i.e., the surface available for O_3 deposition at a microscopic scale.
388 Additional chemical processes that remove O_3 at the interface soil-atmosphere remain
389 possible. For instance, the study performed by Vuolo et al. (2017) indicated that soil O_3
390 deposition increased following slurry application, suggesting a chemical process linked with
391 surface reactivity changes due to the added organic matter or volatile organic compound
392 (VOC) emissions from the slurry. These chemical processes are primarily controlled by
393 temperature, in a purely reactive way (e.g., Cape et al., 2009). Finally, even if O_3 is weakly
394 soluble in water, possible dissolution, diffusion and chemical reaction inside the water films at
395 the soil surface cannot be discarded as suggested by Potier et al. (2015) for O_3 cuticular
396 deposition on wet leaves, implying an impact of e.g., compound concentrations in water films
397 (Potier et al., 2015) or water pH (e.g., Flechard et al., 1999). Understanding these effects
398 could be of particular importance, especially for agroecosystems for which agricultural
399 practices such as ploughing, crushing or organic fertilization can change both soil
400 compaction, organic matter content, and soil surface reactivity.
401

Acknowledgements

This work supported by the European commission through CarboEurope-IP and NitroEurope-IP projects, the French regional funding R2DS (région Ile-de-France), the French-German project PHOTONA (CNRS/INSU/DFG), the French national project Vulnoz (ANR, VMC), the French national project RAVISA (ADEME - French Environment and Energy Management Agency), and partially supported by the program of dissemination and enhancement of the scientific research results of the Catholic University of the Sacred Heart.

The authors gratefully acknowledged all people involved in the measurement campaigns for their assistance in maintenance of the experimental sites, data acquisition and proceeding.

Thanks to Bernard Defranssu, Dominique Tristan, Jean-Pierre de Saint Stéban, Michel Gay, and Benoit Cantaloube for giving access to their fields. Thanks to Michela Scalvenzi and to the Turro's farm for their support.

References

Ahmad Z., Allam I.M., Abdul Aleem B.J., 2000. Effect of environmental factors on the atmospheric corrosion of mild steel in aggressive coastal environment. Anti-Corrosion Methods and Materials 47, 215–225.

Ainsworth E.A., Yendrek C.R., Sitch S., Collins W.J., Emberson L.D., 2012. Ozone on net primary productivity and implications for climate change. Annual Review of Plant Biology 63, 637-661.

Altimir N., Kolari P., Tuovinen J.P., Vesala T., Bäck J., Suni T., Kulmala M., Hari P., 2006. Foliage surface ozone deposition: a role for surface moisture? Biogeosciences 3, 209-228.

Altimir N., Tuovinen J.P., Vesala T., Kulmala M., Hari P., 2004. Measurements of ozone removal by Scots pine shoots: calibration of a stomatal uptake model including the non-stomatal component. Atmospheric Environment 38, 2387-2398.

Aubinet M., Grelle A., Ibrom A., Rannik U., Moncrieff J., Foken T., Kowalski A.S., Martin P.H., Berbigier P., Bernhofer C., Clement R., Elbers J., Granier A., Grunwald T., Morgenstern K., Pilegaard K., Rebmann C., Snijders W., Valentini R., Vesala T., 2000. Estimates of the annual net carbon and water exchange of forests: the EUROFLUX methodology. Advances in Ecological Research 30, 113–175.

Bassin S., Calanca P., Weidinger T., Gerosa G., Fuhrer J., 2004. Modeling seasonal ozone fluxes to grassland and wheat: model improvement, testing, and application. Atmospheric Environment 38, 2349-2359.

Béziat P., Ceschia E., Dedieu G., 2009. Carbon balance of a three crop succession over two cropland sites in South West France. Agricultural and Forest Meteorology 149, 1628-1645.

Booker F., Muntifering R., McGrath M., Burkey K., Decoteau D., Fiscus E., Manning W., Krupa S., Chappelka A., Grantz D., 2009. The ozone component of global change: Potential effects on agricultural and horticultural plant yield, product quality and interactions with invasive species. Journal of Integrative Plant Biology 51, 337-351.

Cape J.N., Hamilton R., Heal M.R., 2009. Reactive uptake of ozone at simulated leaf surfaces: Implications for 'non-stomatal' ozone flux. Atmospheric Environment 43, 1116-1123.

Clifton O.E., Fiore A.M., Munger J.W., Malyshev S., Horowitz L.W., Shevliakova E., Paulot F., Murray L.T., Griffin K.L., 2017. Interannual variability in ozone removal by a temperate deciduous forest. Geophysical Research Letters 44, 542-552.

Coyle M., Nemitz E., Storeton-West R., Fowler D., Cape J.N., 2009. Measurements of ozone deposition to a potato canopy. Agricultural and Forest Meteorology 149, 655-666.

Dizengremel P., Le Thiec D., Bagard M., Jolivet Y., 2008. Ozone risk assessment for plants: Central role of metabolism-dependent changes in reducing power. Environmental Pollution 156, 11-15.

Doherty R.M., Heal M.R., O'Connor F.M., 2017. Climate change impacts on human health over Europe through its effect on air quality. Environmental Healt 16, 33-44.

Emberson L.D., Ashmore M.R., Cambridge H.M., Simpson D., Tuovinen J.P., 2000. Modelling stomatal ozone flux across Europe. Environmental Pollution 109, 403-413.

Fares S., Weber R., Park J.H., Genter D., Karlik J., Goldstein A.H., 2012. Ozone deposition to an orange orchard: Partitioning between stomatal and non-stomatal sinks. Environmental Pollution 169, 258-266.

Felzer B.S., Cronin T., Reilly J.M., Melillo J.M., Wang X., 2007. Impacts of ozone on trees and crops. Comptes Rendus Geoscience 339, 784-798.

Flechard C.R., Fowler D., Sutton M.A., Cape J.N., 1999. A dynamic chemical model of bi-directional ammonia exchange between semi-natural vegetation and the atmosphere. Quarterly Journal of the Royal Meteorological Society 125, 2611-2641.

Fowler D., Pilegaard K., Sutton M.A., Ambus P., Raivonen M., Duyzer J., Simpson D., Fagerli H., Fuzzi S., Schjoerring J.K., Granier C., Neftel A., Isaksen I.S.A, Laj P., Maione M., Monks P.S., Burkhardt J., Daemmgen U., Neirynck J., Personne E., Wichink-Kruit R., Butterbach-Bahl K., Flechard C., Tuovinen J.P., Coyle M., Gerosa G., Loubet B., Altimir N., Gruenhage L., Ammann C., Cieslik S., Paoletti E., Mikkelsen T.N., Ro-Poulsen H., Cellier P., Cape J.N., Horvath L., Loreto F., Niinemets U., Palmer P.I., Rinne J., Misztal P., Nemitz E., Nilsson D., Pryor S., Gallagher M.W., Vesala T., Skiba U., Brüggemann N., Zechmeister-Boltenstern S., Williams J., O'Dowd C., Facchini M.C., de Leeuw G., Flossman A., Chaumerliac N., Erisman J.W., 2009. Atmospheric composition change: Ecosystem-Atmosphere interactions. Atmospheric Environment 43, 5193-5267.

Franz M., Simpson D., Arneth A., Zaehle S., 2017. Development and evaluation of an ozone deposition scheme for coupling to a terrestrial biosphere model. Biogeosciences 14, 45-71.

Freire L.S., Gerken T., Ruiz-Plancarte J., Wei D., Fuentes J.D., Katul G.G., Dias N.L., Acevedo O.C., Chamecki M., 2017. Turbulent mixing and removal of ozone within an Amazon rainforest canopy. Journal of Geophysical Research: Atmospheres 122, 2791-2811.

Garland J.A., 1977. The dry deposition of sulphur dioxide to land and water surface. Proceedings of the Royal Society of London A 354, 245–268.

Güsten H., 1992. A novel ozone sensor for various environmental applications. In: Hudson, R.D. (Ed.), Ozone in the troposphere and stratosphere, Part 1, NASA Conference Publication, vol. 3266. Goddard Space Flight Center, Greenbelt, MD, USA, pp. 127–129.

Güsten H., Heinrich G., Mönnich E., Sprung D., Weppner J., Bakr Ramadan A., Ezz El-Din M.R.M., Ahmed D.M., Hassan G.K.Y., 1996. On-line measurements of ozone surface fluxes: Part II. Surface-level ozone fluxes onto the Sahara desert. Atmospheric Environment 30, 911-918.

Hazucha M.J., Lefohn A.S., 2007. Nonlinearity in human health response to ozone: Experimental laboratory considerations. Atmospheric Environment 41, 4559-4570.

IPCC, 2013. Climate Change 2013: The Physical Science Basis. Contribution of Working Group I to the Fifth Assessment Report of the Intergovernmental Panel on Climate Change [Stocker, T.F., D. Qin, G.-K. Plattner, M. Tignor, S.K. Allen, J. Boschung, A. Nauels, Y. Xia, V. Bex and P.M. Midgley (eds.)]. Cambridge University Press, Cambridge, United Kingdom and New York, NY, USA, 1535 pp.

Ito K., De Leon S.F., Lippmann M., 2005. Associations between ozone and daily mortality: Analysis and meta-analysis. Epidemiology 16, 446-457.

Karnosky D.F., Zak D.R., Pregitzer K.S., Awmack C.S., Bockheim J.G., Dickson R.E., Hendrey G.R., Host G.E., King J.S., Kopper B.J., Kruger E.L., Kubiske M.E., Lindroth R.L., Mattson W.J., McDonald E.P., Noormets A., Oksanen E., Parsons W.F.J., Percy K.E., Podila G.K., Riemenschneider D.E., Sharma P., Thakur R., Sôber A., Sôber J., Jones W.S., Anttonen S., Vapaavuori E., Manlovska B., Heilman W., Isebrands J.G., 2003. Tropospheric O_3 moderates responses of temperate hardwood forests to elevated CO_2: a synthesis of molecular to ecosystem results from the ASPEN face project. Functional Ecology 17, 289-304.

Lamaud E., Loubet B., Irvine M., Stella P., Personne E., Cellier P., 2009. Partitioning of ozone deposition over a developed maize crop between stomatal and non-stomatal uptakes, using eddy-covariance flux measurements and modelling. Agricultural and Forest Meteorology 149, 1385-1396.

Launiainen S., Katul G.G., Grönholm T., Vesala T., 2013. Partitioning ozone fluxes between canopy and forest floor by measurements and a multi-layer model. Agricultural and Forest Meteorology 173, 85-99.

Lee D.S., Holland M.R., Falla N., 1996. The potential impact of ozone on materials in the U.K. Atmospheric Environment 30, 1053-1065.

Lombardozzi D., Levis S., Bonan G., Hess P.G., Sparks J.P., 2015. The influence of chronic ozone exposure on global carbon and water cycles. Journal of Climate 28, 292-305.

Lombardozzi D., Sparks J.P., Bonan G., 2013. Integrating O_3 influences on terrestrial processes: photosynthetic and stomatal response data available for regional and global modeling. Biogeosciences 10, 6815-6831.

Massman W.J., 2004. Toward on ozone standard to protect vegetation based on effective dose: a review of deposition resistances and a possible metric. Atmospheric Environment 38, 2323-2337.

528 Meszaros R., Horvath L., Weidinger T., Neftel A., Nemitz E., Dämmgen U., Cellier P.,
529 Loubet B., 2009. Measurement and modelling ozone fluxes over a cut and fertilized
530 grassland. Biogeosciences 6, 1987-1999.

531 Michou M., Laville P., Serça D., Fotiadi A., Bouchou P., Peuch V.H., 2005. Measured and
532 modeled dry deposition velocities over the ESCOMPTE area. Atmospheric Research
533 74, 89-116.

534 Monks P.S., 2005. Gas-phase radical chemistry in the troposphere. Chemical Society Reviews
535 34, 376-395.

536 Muller J.B.A., Percival C.J., Gallagher M.W., Fowler D., Coyle M., Nemitz E., 2010. Sources
537 of uncertainty in eddy covariance ozone flux measurements made by dry
538 chemiluminescence fast response analysers. Atmospheric Measurement Techniques 3,
539 163–176.

540 Paoletti E., 2005. Ozone slows stomatal response to light and leaf wounding in a
541 Mediterranean evergreen broadleaf, Arbutus unedo. Environmental Pollution 134,
542 439-445.

543 Pennel K.D., 2002. Specific surface area. p. 308-313. In J.H. Dane and G.C. Topp (ed.)
544 Methods of soil analysis. Part 4. SSSA Book Ser. 5. SSSA, Madison, WI.

545 Petersen L.W., Moldrup P., Jacobsen O.H., Rolston D.E., 1996. Relations between specific
546 surface area and soil physical and chemical properties. Soil Science 161, 9-21.

547 Potier E., Ogée J., Jouanguy J., Lamaud E., Stella P., Personne E., Durand B., Mascher N.,
548 Loubet B., 2015. Multilayer modelling of ozone fluxes on winter wheat reveals large
549 deposition on wet senescing leaves. Agricultural and Forest Meteorology 211, 58-71.

550 Scalvenzi M., 2015. Resistenza del suolo nudo alla deposizione di ozono. Thesis of the
551 Master Degree in Physiscs, Università Cattolica del Sacro Cuore, Brescia, Italia,
552 Matricola N. 4109094, 44pp.

553 Schneider M., Goss K.U., 2012. Prediction of the water sorption isotherm in air dry soils.
554 Geoderma, 170, 64-69.

555 Sitch S., Cox P.M., Collins W.J., Huntingford C., 2007. Indirect radiative forcing of climate
556 change through ozone effects on the land-carbon sink. Nature 448, 791-795.

557 Stella P., Lamaud E., Brunet Y., Bonnefond J.M., Loustau, D., Irvine M., 2009. Simultaneous
558 measurements of CO2 and water exchanges over three agroecosystems in South-West
559 France. Biogeosciences 6, 2957–2971.

560 Stella P., Loubet B., Lamaud E., Laville P., Cellier P., 2011b. Ozone deposition onto bare
561 soil: A new parameterisation. Agricultural and Forest Meteorology 151, 669-681.

562 Stella P., Personne E., Lamaud E., Loubet B., Trebs I., Cellier P., 2013. Assessment of the
563 total, stomatal, cuticular, and soil 2 year ozone budgets of an agricultural field with
564 winter wheat and maize crops. Journal of Geophysical Research: Biogeosciences 118,
565 1–13, doi:10.1002/jgrg.20094.

566 Stella P., Personne E., Loubet B., Lamaud E., Ceschia E., Béziat P., Bonnefond J.M., Irvine
567 M., Keravec P., Mascher N., Cellier P., 2011a. Predicting and partitioning ozone
568 fluxes to maize crops from sowing to harvest: the Surfatm-O_3 model. Biogeosciences
569 8, 2869-2886.

570 Stevenson D.S., Dentener F.J. Schultz M.G. Ellingsen K., van Noije T.P.C., Wild O., Zeng
571 G., Amann M., Atherton C.S., Bell N., Bergmann D.J., Bey I., Butler T., Cofala J.,

572 Collins W.J., Derwent R.G., Doherty R.M., Drevet J., Eskes H.J., Fiore A.M., Gauss
573 M., Hauglustaine D.A., Horowitz L.W., Isaksen I.S.A., Krol M.C., Lamarque J.F.,
574 Lawrence M.G., Montanaro V., Müller J.F., Pitari G., Prather M.J., Pyle J.A., Rast S.,
575 Rodriguez J.M., Sanderson M.G., Savage N.H., Shindell D.T., Strahan S.E., Sudo K.,
576 Szopa S., 2006. Multimodel ensemble simulations of present-day and near future
577 tropospheric ozone. Journal of Geophysical Research 111, D08301,
578 doi:10.1029/2005JD006338.

579 Sorimachi A., Sakamoto K., 2007. Laboratory measurement of dry deposition of ozone onto
580 Northern Chinese soil samples. Water, Air, and Soil Pollution: Focus 7, 181-186.

581 Tuovinen J.P., Ashmore M.R., Emberson L.D., Simpson D., 2004. Testing and improving the
582 EMEP ozone deposition module. Atmospheric Environment 38, 2373-2385.

583 Van Pul W.A.J., Jacobs A.F.G., 1994. The conductance of a maize crop and the underlying
584 soil to ozone under various environmental conditions. Boundary-Layer Meteorology
585 69, 83-99.

586 Vickers D., Mahrt L., 1997. Quality Control and Flux Sampling Problems for Tower and
587 Aircraft Data. Journal of Atmospheric and Oceanic Technology 14, 512–526.

588 Vuolo R.M., Loubet B., Mascher N., Gueudet J.C., Durand B., Laville P., Zurfluh O., Ciuraru
589 R., Stella P., Trebs I., 2017. Nitrogen oxides and ozone fluxes from an oilseed-rape
590 management cycle: the influence of cattle slurry application. Biogeosciences 14, 2225-
591 2244.

592 Wesely M.L., Hicks B.B., 2000. A review of the current status of knowledge on dry
593 deposition. Atmospheric Environment 34, 2261–2282.

594 Wilczak J.M., Oncley S.P., Sage S.A., 2001. Sonic anemometer tilt correction algorithms.
595 Boundary-Layer Meteorology 99, 127-150.

596 Wild O., 2007. Modelling the global tropospheric ozone budget: exploring the variability in
597 current models. Atmospheric Chemistry and Physics 7, 2643-2660.

598 Wittig V.E., Ainsworth E.A., Naidu S.L., Karnosky D.F., Long S.P., 2009. Quantifying the
599 impact of current and future tropospheric ozone on tree biomass, growth, physiology
600 and biochemistry: a quantitative meta-analysis. Global Change Biology 15, 396-424.

601 Zhang L., Brook J.R., Vet R., 2002. On ozone dry deposition – with emphasis on non-
602 stomatal uptake and wet canopies. Atmospheric Environment 36, 4787-4799.

603 Zhang L., Vet R., Brook J.R., Legge A.H., 2006. Factors affecting stomatal uptake of ozone
604 by different canopies and a comparison between dose and exposure. Science of the
605 Total Environment 370, 117-132.
606